

Optimum time-to-depth conversion

S. Keydar*, Z. Koren‡, D. Kosloff‡, and E. Landa*

ABSTRACT

Time-to-depth conversion is usually accomplished by converting zero-offset traveltimes, interpreted from a stacked section, to depth using a known velocity field. Time-to-depth conversion is formulated as an iterative procedure producing a depth model which minimizes the differences between zero-offset picked traveltimes and times derived by normal-incidence ray tracing through the model. The input data consist of traveltimes picked from unmigrated stacked sections, as well as assumed interval velocities in each layer. The method can be applied to models with discontinuities such as pinchouts and faults. To illustrate the method, synthetic and field data examples are included.

INTRODUCTION

In seismic exploration, inversion can be defined as the estimation of subsurface physical parameters, such as wave velocity, density, etc. Traveltime tomography uses the traveltimes picked at a range of offsets to determine simultaneously the velocities and interface positions (Bishop et al., 1985). The simplest facet of inversion is the determination of only the geometry of the reflecting interfaces when the seismic velocity is assumed to be known; i.e., time-to-depth conversion. Two widely used methods for time-to-depth conversion are

- (1) Simple multiplication of zero-offset times picked on migrated stack sections by average velocity functions and
- (2) ray map migration (May and Covey, 1981).

The approach outlined below finds a vector of parameters which minimizes some measure of misfit, the objective function $f(\theta)$, where θ contains the parameters of the model (Goldin, 1988). We show that this approach is stable in the presence of velocity and traveltime picking errors and that it permits the use of a priori information about the medium.

Determining the geometry of the subsurface when the velocity is known requires only zero-offset ray tracing and traveltime picking and is much faster and less expensive than tomography. The zero-offset case can be considered a single step in a "poor man's tomography" in which one solves iteratively for interface positions and velocities. The same results can also be achieved by iterating between velocity-depth models and depth migration.

DESCRIPTION OF THE METHOD

We assume that the real medium can be modeled as a sequence of layers separated by interfaces, the location of which must be determined commencing from an initial estimate. Velocity estimation is not considered in this work and, therefore, it is assumed that the interval velocities in each layer are known from well information or from previous interpretation of seismic data. Data consist of picked zero-offset traveltimes of primary reflections, which can be obtained from interpretation of unmigrated stacked sections. Time-to-depth conversion is performed iteratively layer after layer. Despite the obvious drawback of this "top down" strategy, i.e., error accumulation, it has the advantage of allowing a "friendly interaction" between interpreter and computational process.

For a particular layer, the iterative procedure consists of the following three main steps:

- (1) Normal-incidence rays are traced through the initial depth model, producing a set of calculated zero-offset traveltimes.
- (2) The changes in the location of the interface, as defined by the geometrical parameter vector θ , are determined by minimizing the measure of misfit (objective function) between the picked and the computed traveltimes.
- (3) A new location for the interface is obtained by updating the set of geometrical parameters.

The iterative search for the parameter estimates terminates when the objective function is less than a specified

Manuscript received by the Editor January 7, 1988; revised manuscript received January 23, 1989.

*The Institute for Petroleum Research and Geophysics, P.O. Box 2286, Holon 58120, Israel.

‡Department of Geophysics and Planetary Sciences, Tel Aviv University, Tel Aviv 69978, Israel.

© 1989 Society of Exploration Geophysicists. All rights reserved.

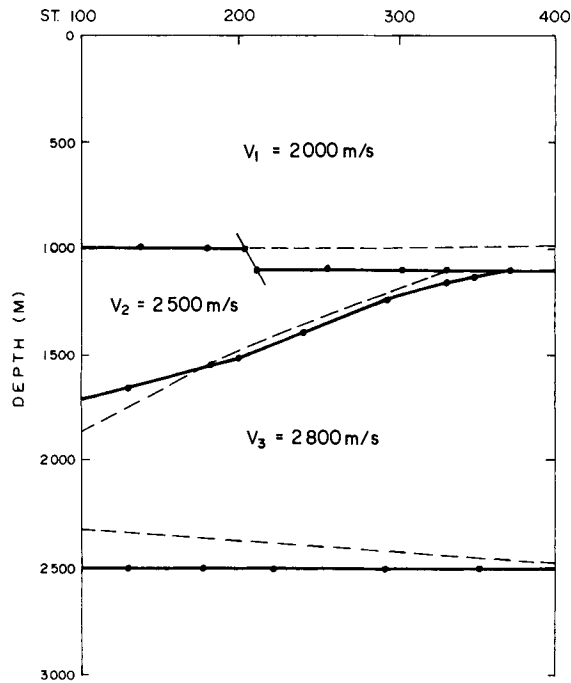


FIG. 1. Synthetic depth model: true model (solid lines) and initial model (dashed lines).

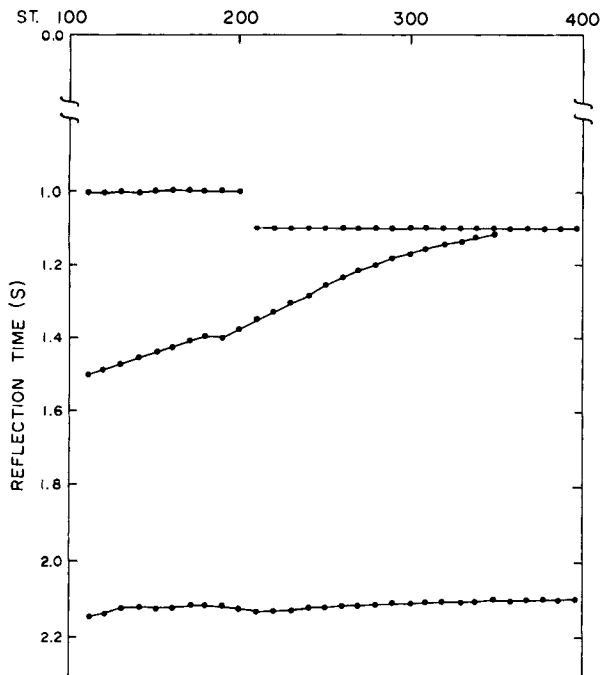


FIG. 2. Time model corresponding to the depth model shown in Figure 1. Dots denote picked traveltimes, and solid lines show the final time model.

value. The convergence of the algorithm depends mainly on the following factors:

- parameterization of the model;
- choice of an objective function;
- method of minimizing the objective function; and
- use of a priori information.

Parameterization of the model

The real medium is replaced by a parametric model in which the reflecting interfaces are described by a vector set of parameters

$$\theta = (X_{11}, Z_{11}, X_{21}, Z_{21}, \dots, X_{n1}, Z_{n1}, X_{12}, Z_{12}, \dots, X_{mn}, Z_{mn}) \quad (1)$$

where X_{mn} , Z_{mn} are, respectively, the horizontal coordinate and the depth of the m th node point along the n th layer.

In our algorithm, the components of the parameter vector are the vertical coordinates of nodes connected by a cubic spline and, optionally, the horizontal coordinates of node points. This type of parameterization permits us to describe different types of structural elements, i.e., faults, pinchouts. When describing an interface, it is sufficient in most cases to estimate the vertical location of node points, while their horizontal coordinates can be fixed. For complex structures, horizontal coordinates are also included in the parameter vector search.

Figure 1 shows the parameterization of a synthetic model with three layers. The dots denote the node points of the interfaces which determine the structural geometry and compose the vector of geometrical parameters θ .

Objective function and minimization algorithm

The squared error between picked and calculated zero-offset traveltimes was chosen as the objective function, i.e.,

$$f(\theta) = \sum_{n=1}^N \sum_{k=1}^N [\hat{t}_{0k}^n - t_{0k}^n(\theta)]^2, \quad (2)$$

where \hat{t}_{0k}^n is the picked time of the n th reflector at the k th midpoint, and $t_{0k}^n(\theta)$ is the modeled zero-offset traveltimes.

In order to minimize the objective function $f(\theta)$, we used the subroutine VA05A from the Harwell Subroutine Library (Powell, 1984). This subroutine is based on a method combining three different algorithms: Newton-Raphson, steepest descent, and Marquardt (for a geophysical example, see Goldman, 1988). We terminated the optimization process when the rms error $\sqrt{f(\theta)}/N$ became less than our threshold value.

A priori information

A priori information on the structure of the medium plays a particularly important role in inversion. One way of using a priori information is to constrain some parameters. Let the goal be to minimize the objective function $f(\theta)$ for a reasonable range of θ_ℓ ,

$$\theta_\ell^{\min} < \theta_\ell < \theta_\ell^{\max},$$

where θ_ℓ^{\min} and θ_ℓ^{\max} are the a priori lower and upper values of the ℓ th parameter θ_ℓ . To solve the constrained problem, the following transformation of the parameter value is carried out (Box, 1966):

$$\theta_\ell^1 = \theta_\ell^{\min} + (\theta_\ell^{\max} - \theta_\ell^{\min}) \sin^2 \theta_\ell. \quad (3)$$

After this transformation, an unconstrained optimum in θ_ℓ^1 space is sought. The periodicity of the optimum solution requires us to select an optimization step small enough to prevent jumping from peak to peak (Box, 1966).

Examples

Figure 1 shows a synthetic depth model with three layers. Zero-offset traveltimes for this model (the dots in Figure 2) are obtained by tracing normal rays through the model. Times, along with the interval velocities, are used as input for the process. The discontinuity in traveltimes between stations 198–200 in the first layer indicates a discontinuity in depth, i.e., the existence of a fault.

The first interface was described by a spline function with eight node points (the closed circles on Figure 1). The unknown parameters are the vertical positions of all of the nodes and the two horizontal locations of the discontinuity, namely, X_3 and X_4 , constrained to be within the range

$$X_{3,4}^{\min} = 180, \quad X_{3,4}^{\max} = 220.$$

The initial model is illustrated in Figure 1 by dashed lines. The program converged to the minimum after six iterations with an rms error of less than 2 ms. Figure 3 illustrates the convergence of the first reflector. For the second layer, the vector of parameters θ consists of seven depth values and the horizontal location of the pinchout, which we restricted to the range 340–380. The program converged after seven iterations, with an rms difference between the input and calculated times of less than 4 ms.

For the last interface, the vector of unknown parameters included only the vertical locations of five node points. The rms

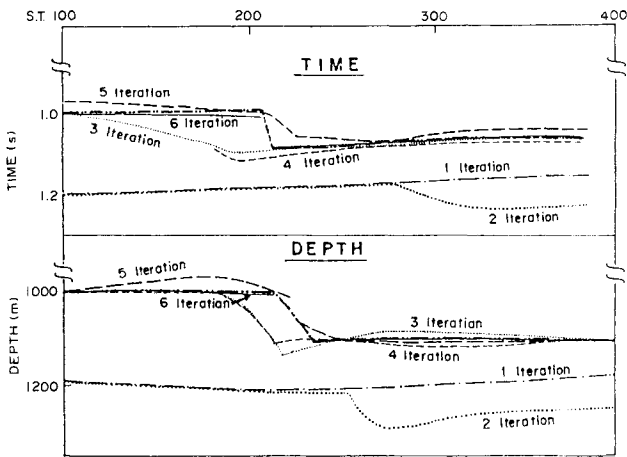


FIG. 3. Convergence of the location of the first reflector.

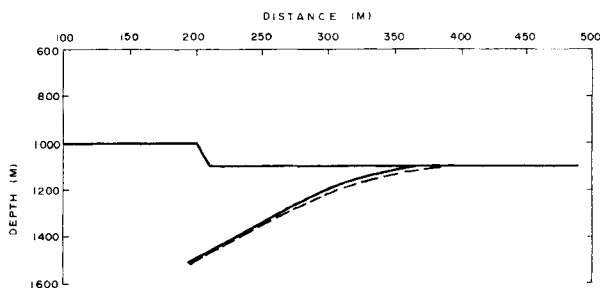


FIG. 4. Depth model (solid lines) and final model (dashed lines) for the second reflector after seven iterations when random noise was added to the picked traveltimes for the second reflector.

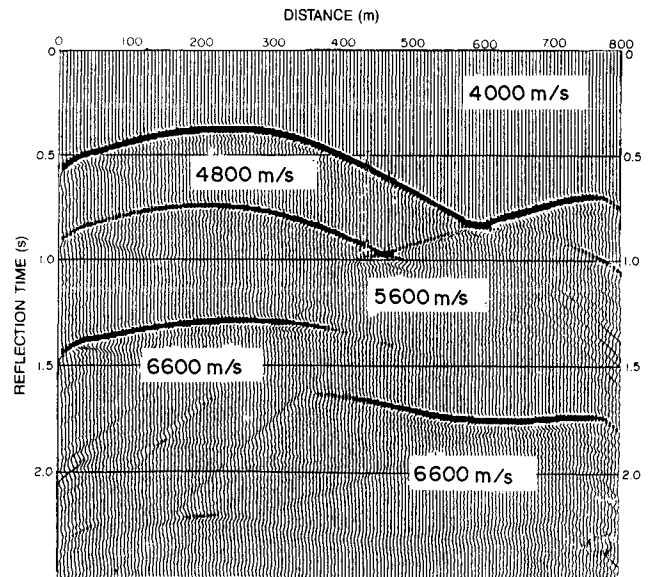


FIG. 5. Time section from a synthetic model obtained using finite-difference modeling.

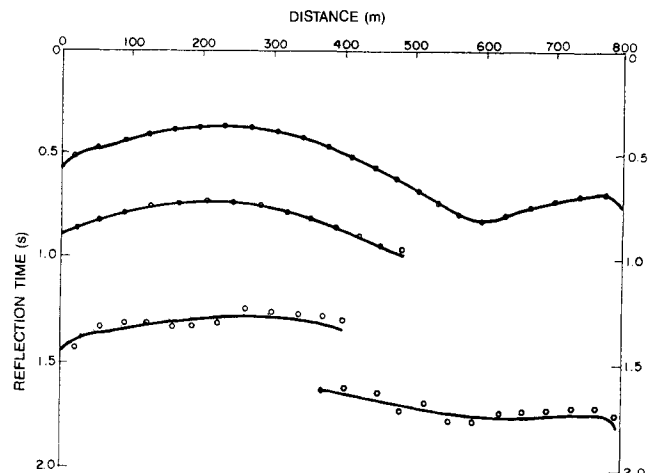


FIG. 6. Traveltimes corresponding to the synthetic time section shown in Figure 5. Dots represent picked times; solid lines represent the calculated times for the final model.

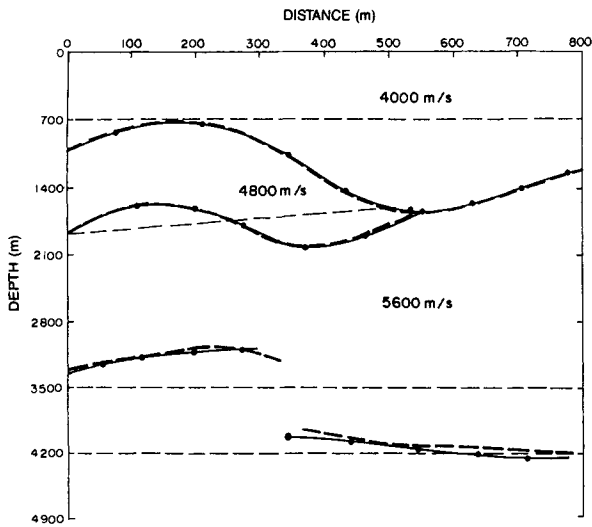


FIG. 7. Velocity-depth model corresponding to the time section shown in Figure 5. The final model corresponds to the thick dashed line, the true model to the solid line, and the initial model to the thin dashed line.

error for this interface was about 2 ms. The final depth model for all three interfaces virtually coincides with the true model.

We illustrate the stability of the proposed method by adding random noise at the rms level of about 8 ms to the picked traveltimes for the second layer. The parameters were the depth location of node points and the horizontal location of the pinchout. The true model and the final model after seven iterations are shown in Figure 4. Although the rms error for the traveltimes was about 10 ms (similar to the noise level), the final model is very close to the true model.

Figure 5 shows a time section from a three-layer model obtained using finite-difference modeling. Figure 6 displays the picked times from only the reflections clearly seen on the time section.

In this example we used a priori information about the presence of a pinchout for the second reflector and a fault for the third. Figure 7 shows a depth section of the model. The search variables for the first layer were the depths of eight node points. The algorithm converged to the final model after six iterations. The rms traveltimes error was about 3 ms. The second interface is defined by six unknown vertical nodes and the horizontal location of the pinchout. We restricted the range of search for the location of the pinchout to between 500 and 600 m. The algorithm converged for the second layer after 15 iterations. The rms traveltimes error was about 4 ms. From Figure 7, we can see that the final model is very close to the

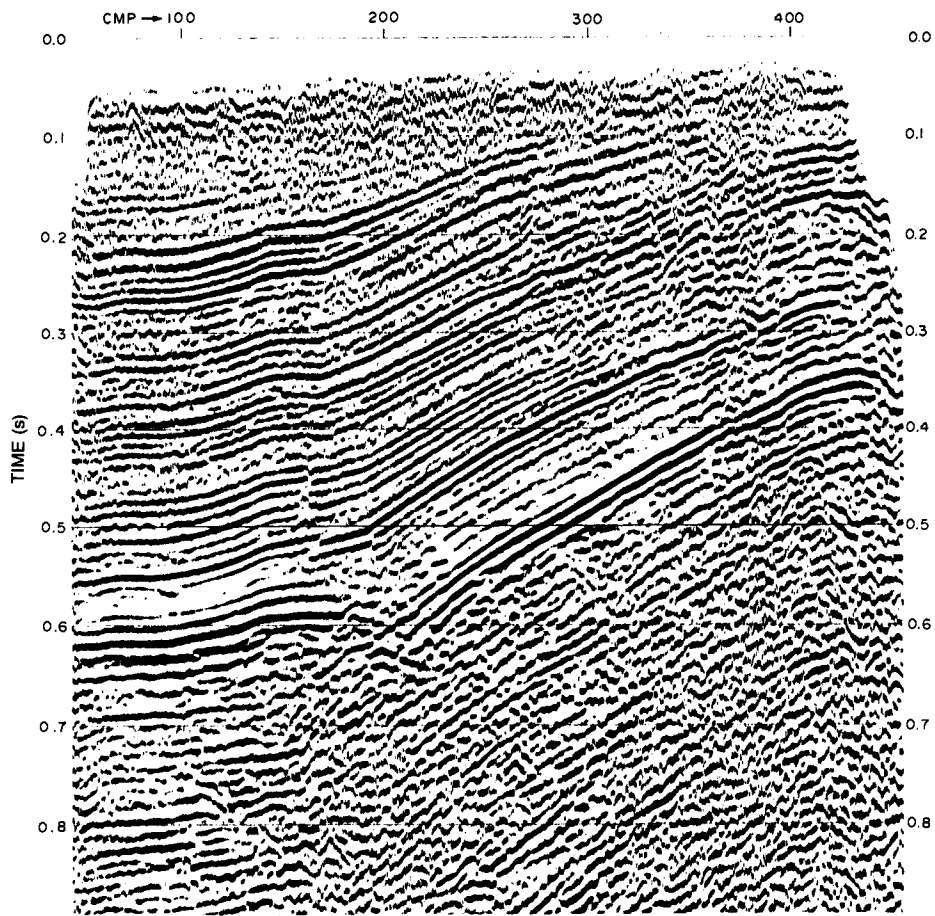


FIG. 8. Stacked seismic section.

true model. The search for the third layer was divided into two steps. First, we looked for the right side of the layer from the discontinuity and then for the left side of the layer. For each side of this layer, the rms traveltimes error was about 8 ms.

Figure 8 shows a stacked section of a real seismic line with 7 m CMP spacing. The picked times obtained by interpreting six clear reflectors are shown in Figure 9. There is a discontinuity in the fifth reflector at CMP 170 and in the sixth reflector at CMP 200. These discontinuities in the time section indicate faults at depth. The layer velocities, which were obtained from well information, are 2200, 1700, 2100, 2230, 2600, and 3300 m/s, respectively. Note the sparseness of the picked times in Figure 9, and their inadequate portrayal of the "plateaus" on reflections 1 through 4 under CMP 160, Figure 8.

Figure 10 represents the depth section, and Figure 9 contains the corresponding traveltimes. For the fifth and sixth reflectors, the parameters included the horizontal locations of the faults. The rms traveltimes errors for the first,

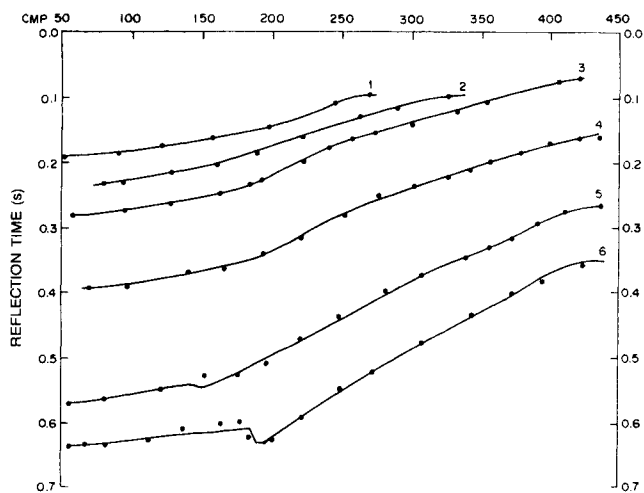


FIG. 9. Time model for the stacked section of Figure 8. Dots represent picked times; solid lines represent calculated times from the final model.

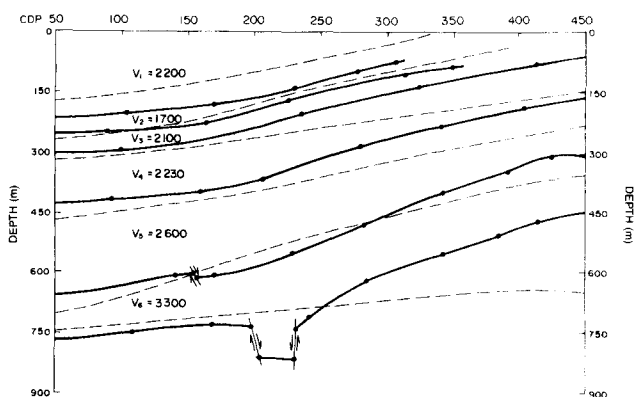


FIG. 10. Depth section corresponding to the stacked section in Figure 8. The final model is represented by solid lines and the initial model by dashed lines.

second, third, and fourth reflectors were less than 3 ms, whereas for the last two reflectors, the error was about 7 ms. The relatively large error can be explained by the complexity of these reflectors.

Computation time for the time-to-depth conversion procedure depends on the number of layers and on the complexity of the model. The real data example required about 30 s of CPU time on an IBM 4341 computer.

Several important points should be stressed: the proposed method is not an automatic procedure for depth model construction, but rather is proposed as a quick interpretation tool for time-to-depth conversion for an interpreter with access to a workstation. Therefore, the final model depends upon the assumption of known velocity, initial guess, location of node points, and a priori information.

CONCLUSIONS

The advantages of the proposed approach are

- good agreement between input times and those calculated for the final depth mode;
- stability in the presence of picking errors;
- validity of the proposed method for both homogeneous and inhomogeneous media;
- use of a priori information in a very convenient form; and
- simple treatment of structurally complex cases.

The method has been successfully tested on synthetic data and real data.

ACKNOWLEDGMENTS

This work was sponsored by the Earth Science Research Administration of the Israel Ministry of Energy and Infrastructure. The authors are grateful to the Institute for Petroleum Research and Geophysics for its permission to publish this paper and to Ilan Bruner for his interpretation of the real data example. The inversion algorithm used the optimization subroutine from the Harwell Subroutine Library.

REFERENCES

- Bishop, T. N., Bube, K. P., Cutler, R. T., Langan, R. T., Love, P. L., Resnick, J. R., Shuey, R. T., Spindler, D. A., and Wyld, H. W., 1985. Tomographic determination of velocity and depth in laterally varying media: *Geophysics*, **50**, 903-925.
- Box, M. J., 1966. A comparison of several current optimization methods and the use of transformations in constrained problems: *Compt. J.*, **9**, 67-77.
- Goldin, S., 1988. Seismic traveltimes inversion: *Soc. Expl. Geoph.*
- Goldman, M., 1988. Transient electromagnetic inversion based on an approximate solution to the forward problem: *Geophysics*, **53**, 118-128.
- May, B. T., and Covey, J. D., 1981. An inverse method for computing geologic structures from seismic reflections—Zero-offset case: *Geophysics*, **46**, 268-287.
- Powell, M. J. D., 1984. Optimization and nonlinear data fitting (subroutine VA05A): Harwell Subroutine Library, U.K. Atomic Energy Authority, Harwell, Oxfordshire.